

Substructure in the ENACS clusters

José M. Solanes¹, Eduard Salvador-Solé², and Guillermo González-Casado³

¹ Departament d'Enginyeria Informàtica, Universitat Rovira i Virgili. Carretera de Salou, s/n; E-43006 Tarragona, Spain.

² Departament d'Astronomia i Meteorologia, Universitat de Barcelona. Av. Diagonal 647; E-08028 Barcelona, Spain.

³ Departament de Matemàtica Aplicada II, Universitat Politècnica de Catalunya. Pau Gargallo 5, E-08028 Barcelona, Spain.
E-mail: solanes@etse.urv.es, eduard@faess0.am.ub.es, guille@coma.upc.es

Received ... / Accepted ...

Abstract. Subclustering is investigated in a set of 67 rich cluster galaxy samples extracted from the ESO Nearby Abell Cluster Survey (ENACS) catalog. We apply four well-known statistical techniques to evaluate the frequency with which substructure occurs. These diagnostics are sensitive to different aspects of the spatial and velocity distribution of galaxies and explore different scales, thus providing complementary tests of subclustering. The skewness and kurtosis of the global radial velocity distributions, useful for judging the normality, and the powerful Δ test of Dressler & Shectman, which measures local deviations from the global kinematics, show that the ENACS clusters exhibit a degree of clumpiness in reasonable agreement with that found in other less homogeneous and smaller cluster datasets. On the other hand, the average two-point correlation function of the projected galaxy distributions reveals that only $\sim 10\%$ of the systems investigated show evidence for substructure at scale lengths smaller than $0.2 h^{-1} \text{Mpc}$. This is much less than in earlier studies based on the Dressler & Shectman's cluster sample. We find indications of a possible systematic deficiency of galaxies at small intergalactic separations in the ENACS clusters.

Key words: methods: data analysis – galaxies: clusters: general – cosmology: observations

1. Introduction

In the last two decades considerable attention has been focused on the study of substructure within rich clusters of galaxies. The importance of subclustering lies in the information it conveys on the properties and dynamics of these systems, which has chief implications for theories of structure formation. A number of authors have developed and applied a variety of methods to evaluate the clumpiness of galaxy clusters both in the optical and X-ray domains (e.g. Geller & Beers 1982; Fitchett & Webster 1987; West et al. 1988; Dressler & Shectman 1988a, hereafter DS88;

West & Bothun 1990; Rhee et al. 1991; Jones & Forman 1992; Mohr et al. 1993; Salvador-Solé et al. 1993a; Bird 1994; Escalera et al. 1994; Serna & Gerbal 1996; Girardi et al. 1997; Gurzadyan & Mazure 1998). Consensus on the results, however, has been frequently hindered by differences on the definition of substructure adopted, on the methodology applied, on the scale used to examine the spatial distribution of the galaxies, and even on the levels of significance chosen to discriminate between real structure and statistical fluctuations.

The debate on the existence of substructure in clusters has been also fueled by the lack of adequate cluster samples to look at the problem. Optical datasets (we will not discuss here X-ray data) which combine both positional and velocity information are essential to determine unambiguously cluster membership and, hence, to eliminate projection uncertainties on the evaluation of subclustering. On the other hand, meaningful estimates of the amount of substructure within rich clusters of galaxies require large catalogs of these systems, free from sampling biases and representative of the total population. Fortunately, a great deal of progress is now being made in this direction thanks to the rapid development of multi-object spectroscopy, which has made possible the emergence of extensive redshift surveys of galaxies in clusters (e.g. Dressler & Shectman 1988b; Teague et al. 1990; Zabludoff et al. 1990; Beers et al. 1991; Malumuth et al. 1992; Yee et al. 1996).

The recently compiled ESO Nearby Abell Cluster Survey (ENACS) catalog (Katgert et al. 1996, 1998) is the result of the last and, by far, most extensive multi-object spectroscopic survey of nearby rich clusters of galaxies. The survey was specifically designed to provide good kinematical data for the construction, in combination with literature data, of a large statistically complete volume-limited sample of rich ACO (Abell, Corwin, & Olowin 1989) clusters in a region of the sky around the South Galactic Pole (Mazure et al. 1996). The catalog contains positions, isophotal (red) R-magnitudes within the 25 mag arcsec⁻² isophote, and redshifts of more than 5600 galaxies in the directions of 107 southern ACO clusters with

richness $R_{\text{ACO}} \geq 1$ and mean redshifts $z \lesssim 0.1$. More importantly, numerous ENACS systems offer the possibility of extracting extended magnitude-limited galaxy samples with a good level of completeness, which is essential for many aspects of the study of the properties of rich clusters, in particular, for detecting substructure.

In this paper, we investigate substructure in a large subset of the ENACS cluster catalog formed by 67 well-sampled systems. Previous studies of subclustering in cluster samples of comparable size have relied on matching separate datasets and thus could not attain a high degree of homogeneity. We apply to our clusters a variety of well-known and complementary statistical tests for substructure, which analyze information from the projected positions of the galaxies and/or their radial velocities. Our aim is to evaluate the fractions of clumpy ENACS systems implied by the different techniques and to compare them with results from former studies relying on the same substructure diagnostics. We begin by discussing in Sect. 2 the selection of our cluster sample. Subclustering is investigated in Sect. 3 by means of three powerful classical tests which examine the velocity dimension of the cluster data. The moment-based coefficients of skewness and kurtosis are used to detect deviations from Gaussianity in the velocity distributions, which are often correlated with the presence of substructure in galaxy clusters. We also apply the 3D diagnostic for substructure defined in DS88, known as the Δ test, to search for localized spatial-velocity correlations. These statistics are complemented in Sect. 4 by the two-point correlation formalism (Salvador-Solé et al. 1993b; hereafter Sa93), which is used to look for signs of small-scale subclustering in the two dimensional galaxy distributions. Section 5 contains a summary and discussion of our results.

2. The cluster sample

A total of 220 compact redshift systems with at least 4 member galaxies and redshifts up to $z \lesssim 0.1$ have been identified in the ENACS catalog by Katgert et al. (1996; see their Table 6). These systems were defined by grouping all the galaxies separated by a gap of less than 1000 km s^{-1} from its nearest neighbor in velocity space along the directions of the clusters targeted in the course of the project. Membership for the systems with at least 50 galaxies in the original compilation suffered further refinement through the removal of interlopers (i.e. galaxies that are unlikely system members but that were not excluded by the 1000 km s^{-1} fixed-gap criterion) by means of an iterative procedure that relies on an estimate of the mass profile of the system (see Mazure et al. 1996 for details).

The completeness (number of redshifts obtained vs number of galaxies observed) of the ENACS data varies from one sample to another and as a function of apparent magnitude. Katgert et al. (1998) show that the completeness of the entire catalog reaches a maximum of about 80%

at intermediate magnitudes and stays approximately constant up to $R_{25} = 17$. Most of the ENACS clusters have indeed its maximum completeness (which oscillates between 60% and 90%) at about this limit (Katgert et al. 1996). At the bright end, the completeness decreases slightly due to the low central surface brightness of some of the brightest galaxies with sizes larger than the diameter of the Optopus fibers, while for $R_{25} \gtrsim 17$ it falls abruptly due to the smaller S/N-ratio of the spectra of the fainter galaxies. According to these results, and in order to deal with galaxy samples with the maximum level of completeness, we have removed from the ENACS systems all the galaxies with an R_{25} magnitude larger than 17. Furthermore, to obtain minimally robust results we have excluded from the present analysis those systems with less than 20 galaxies left after the trimming in apparent brightness. These restrictions lead to a final cluster dataset of 67 compact redshift systems with a good level of completeness in magnitude and containing a minimum of 20 member galaxies each.

All but one (Abell 3559) of the 29 clusters for which several Optopus plates were taken (within each plate spectroscopy was attempted only for the 50 brightest galaxies) are included in our cluster sample. These “multiple-plate” clusters identify the richest and more compact in redshift space systems surveyed. One of these, the “double” cluster Abell 548, has been separated into its SW and NE components (see e.g. Davis et al. 1995), hereafter referred to as A0548W and A0548E, respectively. Our database also includes 3 large secondary systems seen in projection in the fields of two of the 29 multiple-plate clusters: the systems in the foreground and in the background of Abell 151, designated here as A0151F and A0151B, respectively, and the background galaxy concentration seen in the field of Abell 2819, designated here as A2819B. The remaining 35 systems are “single-plate” clusters for which a unique Optopus field was defined (they all have, then, $N \leq 50$). These systems are identified in tables and figures by an asterisk.

Detailed information about each one of the systems selected, including robust estimates of their main physical properties, can be found along the series of ENACS papers, especially in the articles cited in this section.

3. Substructure diagnostics relying on velocity data

3.1. Description of the tests

To detect deviations from Gaussianity in the cluster’s velocity distributions, we use the classical coefficients of skewness and kurtosis, which have been shown to offer greater sensitivity than other techniques based on the order statistics or the gaps of the datasets (see e.g. Bird & Beers 1993). The coefficient of skewness, which is the third

moment about the mean, measures the asymmetry of the distribution. It is computed as

$$S = \frac{1}{\sigma^3} \left[\frac{1}{N} \sum_{i=1}^N (v_i - \bar{v})^3 \right], \quad (1)$$

with \bar{v} and σ the mean velocity and standard deviation determined from the observed line-of-sight velocities v_i of the N cluster members. A positive (negative) value of S implies that the distribution is skewed toward values greater (less) than the mean.

The kurtosis is the fourth moment about the mean and measures the relative population of the tails of the distribution compared to its central region. Since the kurtosis of a normal distribution is expected to be equal to 3, the kurtosis coefficient is usually defined to be neutrally elongated for a Gaussian, in the form

$$K = \frac{1}{\sigma^4} \left[\frac{1}{N} \sum_{i=1}^N (v_i - \bar{v})^4 \right] - 3. \quad (2)$$

Positive values of K indicate distributions peakier than Gaussian and/or with heavier tails, while negative values reflect boxy distributions that are flatter than Gaussian and/or with lighter tails. The significance of the empirical values of the above two coefficients is simply given by the probability that they are obtained by chance in a normal distribution.

Together with the above normality tests, we apply also the Δ test of DS88, which is a simple and powerful 3D substructure diagnostic designed to look for local correlations between galaxy positions and velocity that differ significantly from the overall distribution within the cluster. It is based on the comparison of a local estimate of the velocity mean \bar{v}_1 and dispersion σ_1 for each galaxy with measured radial velocity, with the values of these same kinematical parameters for the entire sample. The presence of substructure is quantified by means of a sole statistic defined from the sum of the local kinematic deviations δ_i over the N cluster members, in the form (Bird 1994)

$$\Delta = \sum_{i=1}^N \delta_i = \sum_{i=1}^N \left[\frac{\text{nint}(\sqrt{N}) + 1}{\sigma^2} ((\bar{v}_{1,i} - \bar{v})^2 + (\sigma_{1,i} - \sigma)^2) \right]^{\frac{1}{2}}, \quad (3)$$

with $\text{nint}(x)$ standing for the integer nearest to x . To avoid the formulation of any hypothesis on the form of the velocity distribution of the parent population, the Δ statistic is calibrated by means of Monte-Carlo simulations (we perform 1000 per cluster) that randomly shuffle the velocities of the cluster members while keeping their observed positions fixed. In this way any existing local correlation between velocities and positions is destroyed. The probability of the null hypothesis that there are no such correlations is given in terms of the fraction of simulated clusters

Table 1. Results of the kinematical substructure tests

Cluster (1)	N (2)	$p(S)$ (3)	$p(K)$ (4)	$p(\Delta)$ (5)
A0013*	37	0.386	0.024	0.035
A0087*	22	0.450	0.263	0.106
A0118*	28	0.332	0.197	0.201
A0119	87	0.245	0.601	0.681
A0151F	23	0.245	0.270	0.848
A0151	42	0.280	0.114	0.669
A0151B	21	0.230	0.385	0.008
A0168	74	0.178	0.024	0.287
A0229*	23	0.252	0.167	0.018
A0295*	26	0.202	0.566	0.544
A0367*	23	0.414	0.048	0.653
A0514	63	0.132	0.175	0.214
A0548W	109	0.128	0.272	<0.001
A0548E	100	0.171	0.051	<0.001
A0754*	39	0.099	0.309	0.351
A0957*	34	0.495	0.291	0.034
A0978	57	0.006	0.006	0.004
A1069*	35	0.014	0.676	0.208
A1809*	30	0.107	0.296	0.563
A2040*	37	0.248	0.362	0.107
A2048*	23	0.229	0.311	0.969
A2052*	35	0.009	0.028	0.542
A2401*	23	0.315	0.647	0.001
A2569*	30	0.216	0.416	0.021
A2717	28	0.294	0.173	0.373
A2734	45	0.283	0.415	0.140
A2755*	22	0.196	0.264	0.011
A2799*	36	0.162	0.160	0.356
A2800*	32	0.416	0.068	0.297
A2819	40	0.047	0.088	0.631
A2819B	36	0.012	0.013	0.322
A2854*	22	0.061	0.357	0.644
A2911*	22	0.261	0.089	0.055
A3093*	20	0.460	0.385	0.479
A3094	46	0.329	0.043	0.004
A3111*	35	0.057	0.351	0.072
A3112	67	0.282	0.243	0.280
A3122	62	0.391	0.441	0.039
A3128	152	0.224	0.108	<0.001
A3151*	29	0.072	0.577	0.074
A3158	95	0.468	0.136	0.393
A3194*	32	0.378	0.009	0.010
A3202*	27	0.254	0.108	0.052
A3223	64	0.000	0.004	0.162
A3341	48	0.404	0.007	0.910
A3354	48	0.169	0.424	<0.001
A3365*	28	0.221	0.002	0.005
A3528*	28	0.192	0.039	0.277
A3558	40	0.329	0.146	0.186
A3562	52	0.025	0.253	0.003
A3651	78	0.446	0.254	0.026
A3667	102	0.249	0.581	0.199
A3691*	31	0.116	0.221	0.203
A3695	67	0.220	0.408	<0.001
A3705*	22	0.299	0.175	0.044

Table 1. (continued)

Cluster (1)	N (2)	$p(S)$ (3)	$p(K)$ (4)	$p(\Delta)$ (5)
A3733*	41	0.140	0.558	0.409
A3744	59	0.022	0.166	0.153
A3764*	33	0.037	0.043	0.759
A3806	97	0.020	0.222	0.058
A3809	80	0.109	0.204	0.274
A3822	68	0.117	0.268	0.038
A3825	45	0.194	0.424	0.160
A3864*	32	0.328	0.576	0.935
A3879	33	0.099	0.003	0.452
A3921*	32	0.221	0.022	0.767
A4008*	24	0.220	0.268	0.407
A4010*	27	0.259	0.515	0.930

for which their cumulative deviation is smaller than the observed value.

3.2. Results

Table 1 summarizes, for each one of the 67 magnitude-limited galaxy samples defined in Sect. 2, the number of galaxies N meeting the selection criteria and the probabilities that the empirical values of the three statistics described above could have arisen by chance (the smaller the quoted value the more significant is the departure from the null hypothesis). At the 5% significance level (in this section all results will be referred to this level of significance) about 30% (20 of 67) of the systems exhibit a non-Gaussian velocity distribution according to at least one of the two normality tests. This is a little small fraction if compared with the results of previous studies by West & Bothun (1990), Bird & Beers (1993), and Bird (1994), in which $\sim 40\% - 50\%$ of the clusters investigated had radial velocity distributions with non-normal values of the skewness and/or kurtosis. The discrepancies, however, are not statistically significant and point to possible biases towards the inclusion of clumpy systems in former cluster datasets (see, for instance, the selection criteria applied by Dressler & Shectman 1988b). The normality tests do not detect either significant differences between the single- and multiple-plate subsets, which indicate frequencies of rejection of the Gaussian hypothesis, 26% (9/35) and 34% (11/32) respectively, fully compatible within the statistical uncertainties.

On the other hand, 31% (21/67) of our clusters are found to show substructure according to the Δ test. In a recent investigation of the kinematics and spatial distribution of the Emission-Line Galaxies (ELG) in clusters, Biviano et al. (1997) have applied this same test to the 25 ENACS systems with $N \geq 50$ that contain at least

one ELG, finding evidence for substructure in $\sim 40\%$ of the cases. As was to be expected, this value is in excellent agreement with the 38% (12/32) of the multiple-plate systems which demonstrate substructure in our dataset. Previous analysis of subclustering also relying on the Δ statistic by Escalera et al. (1994) and Bird (1994) claim similar percentages of clumpy systems, 38% (6/16) and 44% (11/25) respectively, while the fraction quoted in the original work by DS88 is somewhat higher, 53% (8/15), but still compatible with the other results within the statistical uncertainties. We emphasize, however, that none of the preceding works paid attention to the completeness in magnitude of the galaxy samples under scrutiny. As in the case of the Gaussianity tests, we do not find significant differences between the fractions of substructured single-plate systems (9/35) and multiple-plate ones (12/32) indicated by the Δ statistic.

4. The average two-point correlation function

4.1. Definition and practical implementation

The average two-point correlation function $\bar{\xi}$ (see Sa93 for details) was introduced for the statistical characterization of subclustering in inhomogeneous systems with isotropy around one single point. Given a circularly symmetric galaxy cluster, this statistic can be calculated exactly as the usual two-point correlation function in the homogeneous and isotropic case through the expression

$$\bar{\xi}(s) = \frac{(\rho * \rho)(s) - (n * n)(s)}{(n * n)(s)} - \frac{1}{N}, \quad (4)$$

with ρ some continuous function approximating the observed number density distribution of galaxies, and n the mean radial number density profile estimated from the azimuthal average of ρ . Notice that, contrarily to ρ , n is insensitive to the existence of correlation in galaxy positions. The additive constant $1/N$ in Eq. (4) corrects for the negative bias caused by the fact that each cluster galaxy chosen at random has *only* $N - 1$ neighbors, one less than the number expected for a fully random process.

The autocorrelation products $\rho * \rho$ and $n * n$ are computed via the sequence of transformations (see also Salvador-Solé et al. 1993a)

$$(\rho * \rho)(s) = \mathcal{F}_1 \circ \mathcal{A} \left[\mathcal{A} \circ \mathcal{F}_1^{-1} \left(2 \int_s^\infty P(x) dx \right) \right], \quad (5)$$

and

$$(n * n)(s) = \mathcal{F}_1 \circ \mathcal{A} \left[\mathcal{A} \circ \mathcal{F}_1^{-1} \left(\int_s^\infty \Pi(x) dx \right) \right]^2, \quad (6)$$

which rely, respectively, on the calculation of the cumulative forms of $P(s) ds$, the number of pairs of galaxies with observed separation between s and $s + ds$ among the $N(N - 1)/2$ galaxy pairs obtained from the cluster sample, and of $\Pi(s) ds$, the number of galaxies at projected

Table 2. Characteristics of the 67 clusters

Cluster	Barycenter coords. RA (B1950) Dec	e	θ (rad)	r_{eq} ($h^{-1}\text{Mpc}$)	N_c
(1)	(2)	(3)	(4)	(5)	(6)
A0013*	00 ^h 11 ^m 03 ^s .0, −19°47′40″	0.17	−0.26	0.42	20
A0087*	00 ^h 40 ^m 15 ^s .8, −10°05′01″	0.80	0.57	0.54	20
A0118*	00 ^h 52 ^m 45 ^s .6, −26°38′27″	0.80	0.83	1.17	28
A0119	00 ^h 53 ^m 39 ^s .6, −01°30′39″	0.84	1.39	0.92	81
A0151F	01 ^h 06 ^m 24 ^s .3, −16°14′50″	0.58	−0.94	0.19	8
A0151	01 ^h 06 ^m 44 ^s .4, −15°45′25″	0.32	−0.48	0.68	33
A0151B	01 ^h 06 ^m 12 ^s .3, −15°51′07″	0.50	0.69	1.25	17
A0168	01 ^h 12 ^m 31 ^s .0, 00°02′26″	0.49	−1.07	0.76	62
A0229*	01 ^h 37 ^m 03 ^s .5, −03°55′14″	0.39	−0.33	0.51	11
A0295*	01 ^h 59 ^m 34 ^s .5, −01°19′20″	0.80	0.32	0.36	21
A0367*	02 ^h 34 ^m 23 ^s .6, −19°33′59″	0.64	−0.55	0.89	19
A0514	04 ^h 45 ^m 56 ^s .8, −20°35′49″	0.58	−0.37	0.97	56
A0548W	05 ^h 42 ^m 53 ^s .0, −25°55′35″	0.65	0.74	0.90	82
A0548E	05 ^h 46 ^m 00 ^s .9, −25°32′32″	0.96	0.49	1.12	98
A0754*	09 ^h 06 ^m 19 ^s .7, −09°25′47″	0.49	−0.23	0.31	21
A0957*	10 ^h 11 ^m 09 ^s .5, 00°38′47″	0.22	0.07	0.23	23
A0978	10 ^h 18 ^m 00 ^s .5, −06°21′40″	0.27	−1.40	0.78	48
A1069*	10 ^h 37 ^m 13 ^s .9, −08°21′54″	0.40	−1.43	0.46	25
A1809*	13 ^h 50 ^m 31 ^s .4, 05°23′06″	0.53	1.01	0.72	28
A2040*	15 ^h 10 ^m 24 ^s .2, 07°36′58″	0.88	−0.13	0.44	31
A2048*	15 ^h 12 ^m 44 ^s .0, 04°33′15″	0.60	−1.51	0.75	20
A2052*	15 ^h 14 ^m 23 ^s .7, 07°15′25″	0.73	1.40	0.33	28
A2401*	21 ^h 55 ^m 50 ^s .0, −20°17′58″	0.91	0.40	0.41	19
A2569*	23 ^h 15 ^m 09 ^s .9, −13°06′12″	0.95	−1.12	0.66	22
A2717	00 ^h 00 ^m 05 ^s .3, −36°08′00″	0.46	−0.12	0.67	20
A2734	00 ^h 08 ^m 46 ^s .1, −29°06′36″	0.52	0.03	0.90	37
A2755*	00 ^h 15 ^m 08 ^s .7, −35°25′48″	0.60	−0.14	0.78	15
A2799*	00 ^h 34 ^m 55 ^s .9, −39°27′15″	0.48	0.57	0.67	32
A2800*	00 ^h 35 ^m 35 ^s .6, −25°24′26″	0.51	1.12	0.44	18
A2819	00 ^h 43 ^m 40 ^s .5, −63°49′35″	0.31	0.26	1.30	33
A2819B	00 ^h 43 ^m 38 ^s .5, −63°50′59″	0.54	−0.15	2.05	34
A2854*	00 ^h 58 ^m 23 ^s .1, −50°46′39″	0.40	−1.05	0.43	14
A2911*	01 ^h 23 ^m 57 ^s .4, −38°11′37″	0.65	−0.50	0.33	10
A3093*	03 ^h 09 ^m 18 ^s .1, −47°35′55″	0.19	−0.23	0.55	12
A3094	03 ^h 09 ^m 51 ^s .8, −27°09′29″	0.38	−0.48	0.99	39
A3111*	03 ^h 15 ^m 49 ^s .6, −45°52′04″	0.69	−0.84	0.73	26
A3112	03 ^h 16 ^m 18 ^s .6, −44°27′07″	0.88	0.40	1.60	65
A3122	03 ^h 20 ^m 35 ^s .8, −41°30′45″	0.65	0.14	0.86	39
A3128	03 ^h 28 ^m 52 ^s .7, −52°48′57″	0.61	0.45	2.19	152
A3151*	03 ^h 38 ^m 30 ^s .7, −28°51′41″	0.28	0.11	0.31	22
A3158	03 ^h 41 ^m 13 ^s .6, −53°47′53″	0.73	0.21	1.34	77
A3194*	03 ^h 57 ^m 04 ^s .4, −30°19′01″	0.23	1.12	0.39	14
A3202*	03 ^h 59 ^m 30 ^s .0, −53°48′56″	0.38	−0.01	0.56	19
A3223	04 ^h 06 ^m 16 ^s .7, −31°02′09″	0.57	1.25	1.02	53
A3341	05 ^h 23 ^m 44 ^s .2, −31°34′58″	0.70	1.30	0.70	45
A3354	05 ^h 32 ^m 45 ^s .0, −28°36′08″	0.43	−1.23	1.09	43
A3365*	05 ^h 46 ^m 07 ^s .9, −21°55′57″	0.34	0.53	0.59	22
A3528*	12 ^h 51 ^m 44 ^s .1, −28°45′03″	0.84	0.91	0.33	15
A3558	13 ^h 25 ^m 49 ^s .7, −31°13′26″	0.62	−0.89	0.85	34
A3562	13 ^h 28 ^m 28 ^s .0, −31°26′09″	0.55	−0.69	0.57	23
A3651	19 ^h 48 ^m 15 ^s .1, −55°12′31″	0.40	−0.10	1.12	43
A3667	20 ^h 07 ^m 53 ^s .8, −56°56′59″	0.34	−0.61	1.50	87
A3691*	20 ^h 31 ^m 02 ^s .5, −38°12′57″	0.55	−1.36	0.64	21

Table 2. (continued)

Cluster	Barycenter coords. RA (B1950) Dec	e	θ (rad)	r_{eq} (h^{-1} Mpc)	N_c
(1)	(2)	(3)	(4)	(5)	(6)
A3695	20 ^h 31 ^m 39 ^s .8, −36°00′12″	0.47	−1.19	1.34	47
A3705*	20 ^h 38 ^m 40 ^s .0, −35°23′55″	0.23	0.36	0.45	13
A3733*	20 ^h 58 ^m 52 ^s .3, −28°18′41″	0.29	−1.50	0.28	19
A3744	21 ^h 04 ^m 22 ^s .6, −25°41′35″	0.83	0.34	0.62	46
A3764*	21 ^h 22 ^m 58 ^s .4, −35°01′09″	0.09	−1.15	0.24	11
A3806	21 ^h 41 ^m 38 ^s .2, −57°24′42″	0.31	−0.26	1.85	79
A3809	21 ^h 44 ^m 02 ^s .8, −44°10′58″	0.40	−0.12	0.97	59
A3822	21 ^h 50 ^m 22 ^s .7, −58°03′14″	0.40	−0.13	2.05	61
A3825	21 ^h 54 ^m 45 ^s .8, −60°37′07″	0.54	−0.32	1.26	34
A3864*	22 ^h 16 ^m 50 ^s .4, −52°45′28″	0.34	−0.53	1.13	26
A3879	22 ^h 24 ^m 00 ^s .0, −69°14′03″	0.55	−0.11	0.93	24
A3921*	22 ^h 46 ^m 30 ^s .6, −64°40′33″	0.39	0.00	1.43	27
A4008*	23 ^h 27 ^m 36 ^s .9, −39°34′04″	0.76	1.20	0.52	18
A4010*	23 ^h 28 ^m 49 ^s .6, −36°47′31″	0.42	0.36	0.72	22

distances between s and $s + ds$ from the center of symmetry of the galaxy distribution. In Eqs. (5) and (6) \mathcal{F}_1 and \mathcal{A} stand, respectively, for the one-dimensional Fourier and Abel transformations, while the symbol “ \circ ” denotes the composition of functions. From the latter two equations it is readily apparent that the numerical estimate of ξ is independent of the bin size used for the integrals $\int_s^\infty P(x) dx$ and $\int_s^\infty \Pi(x) dx$, which merely determines the sampling interval of the solution, so there are no lower limits on the size of the subclumps that can be detected (nor a priori assumptions on their possible number and shapes are required). Nonetheless, it is advisable to attenuate the statistical noise of $\xi(s)$ at galactic scales (Sa93). Thus, we apply a low-passband hamming filter leading to a final resolution length of $0.05 h^{-1}$ Mpc. Notice also that the use of the cumulative forms of the distributions $P(s)$ and $\Pi(s)$ makes this statistic particularly well suited for galaxy samples containing a small number of objects.

The statistical significance of substructure for each cluster is obtained by checking the null hypothesis that the observed $\rho(s)$ arises from a Poissonian realization of an unknown theoretical density profile, which is approximated by $n(s)$. In practice, this translates to a comparison between the empirical function given by Eq. (4) with the mean and one standard deviation of the same function obtained from a large number of Poissonian cluster simulations (i.e. both the radius and the azimuthal angle of each galaxy are chosen at random) that reproduce the profile $n(s)$.

4.2. Results

In order to apply this diagnostic, circularly symmetric galaxy subsamples have been extracted from our dataset

by means of a three-step procedure. The first step consists in the determination of the system barycenter through an iterative process that uses only those galaxies located inside the maximum circle, around the centroid obtained in the previous iteration, inscribed within the limits of the surveyed field. This procedure mitigates any incompleteness in position caused by the spatial filters used in the data acquisition and, when several structures are present in the same region, tends to focus on the main subsystem. A second iterative process calculates the system ellipticity e , which is assumed to be homologous, and the orientation θ of its major axis. Analogously to the barycenter determination, galaxies located in incomplete (elliptical) spatial bins around the barycenter are excluded from the calculations. Finally, circular symmetry is ensured by contracting the galaxy coordinates along the semimajor axis by \sqrt{e} and expanding the semiminor-axis coordinates by the inverse of this same factor. In this manner, we take into account elongation effects that might artificially indicate clumpiness, while any true signal of subclustering is preserved.

Table 2 lists, system by system, the barycenter coordinates, the values of the parameters e and θ (relative to the WE direction)¹, the equivalent radius r_{eq} (i.e. the radius of a circle with an area equal to the maximum elliptical isopleth contour) in h^{-1} Mpc, and the number of galaxies N_c included in the circularly symmetric subsamples. Physical units have been inferred from the cosmological distances of the clusters, which are calculated by correcting their mean heliocentric redshifts to the Cosmic Mi-

¹ Adami et al. (1998) have also inferred these parameters for a number of clusters in this list from Maximum-Likelihood fits to the COSMOS data, obtaining compatible results.

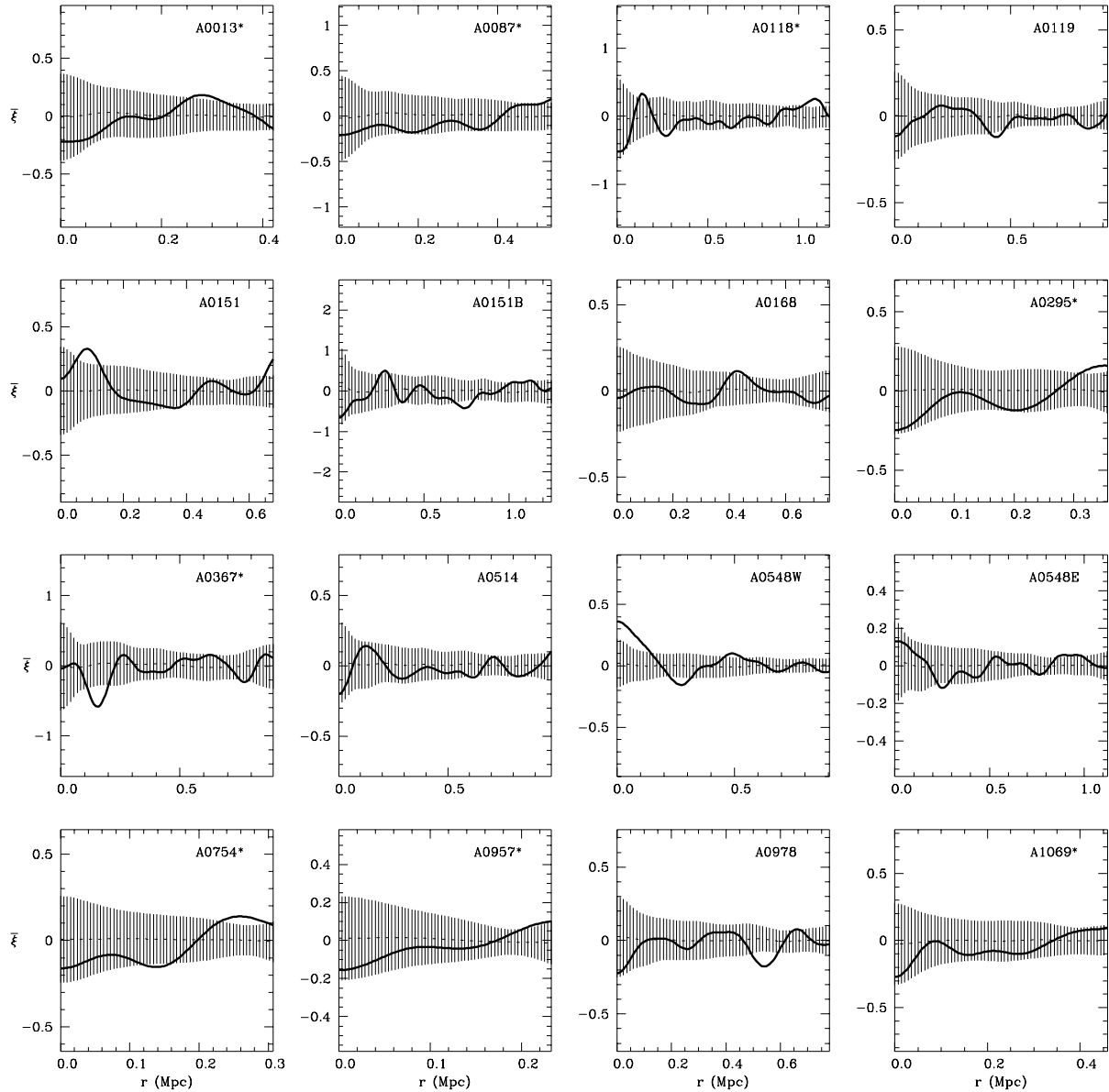


Fig. 1. Average two-point correlation function for the 59 circularly symmetric galaxy samples with $N_c \geq 15$ compared with the mean solution (dashed line) and 1σ -error (vertical solid lines) obtained from 200 Poissonian simulations of each cluster. The spatial resolution is $0.05 h^{-1}\text{Mpc}$.

crowave Background rest frame according to the dipole measured by Kogut et al. (1993).

To minimize small-number effects, the calculation of the average two-point correlation function was restricted to the 59 circularly symmetric galaxy subsamples with 15 or more objects. The results are depicted in Fig. 1, together with the mean solutions and 1σ -errors resulting from 200 Poissonian realizations of each cluster. These plots show that only 6 systems, A0151, A0548W, A2755*, A3128, A3223, and A3879, have a strictly positive signal raising above the noise at separations smaller than

$0.2 h^{-1}\text{Mpc}$ (as in Sa93, we consider the presence of central maxima reaching at least the 1σ level as indicative of small-scale subclustering). Two other systems, A0118* and A3691*, exhibit also a positive departure of more than 1σ at these small scales, but have negative central values of $\bar{\xi}$. Indeed, about three fourths (46 of 59) of the clusters in our sample present negative central signals which, in 15 cases, even go over 1σ .

These results are in notorious contradistinction with those inferred in Sa93 from the analysis of 14 of the 15 Dressler & Shectman's (1988b) clusters (Abell 548 was

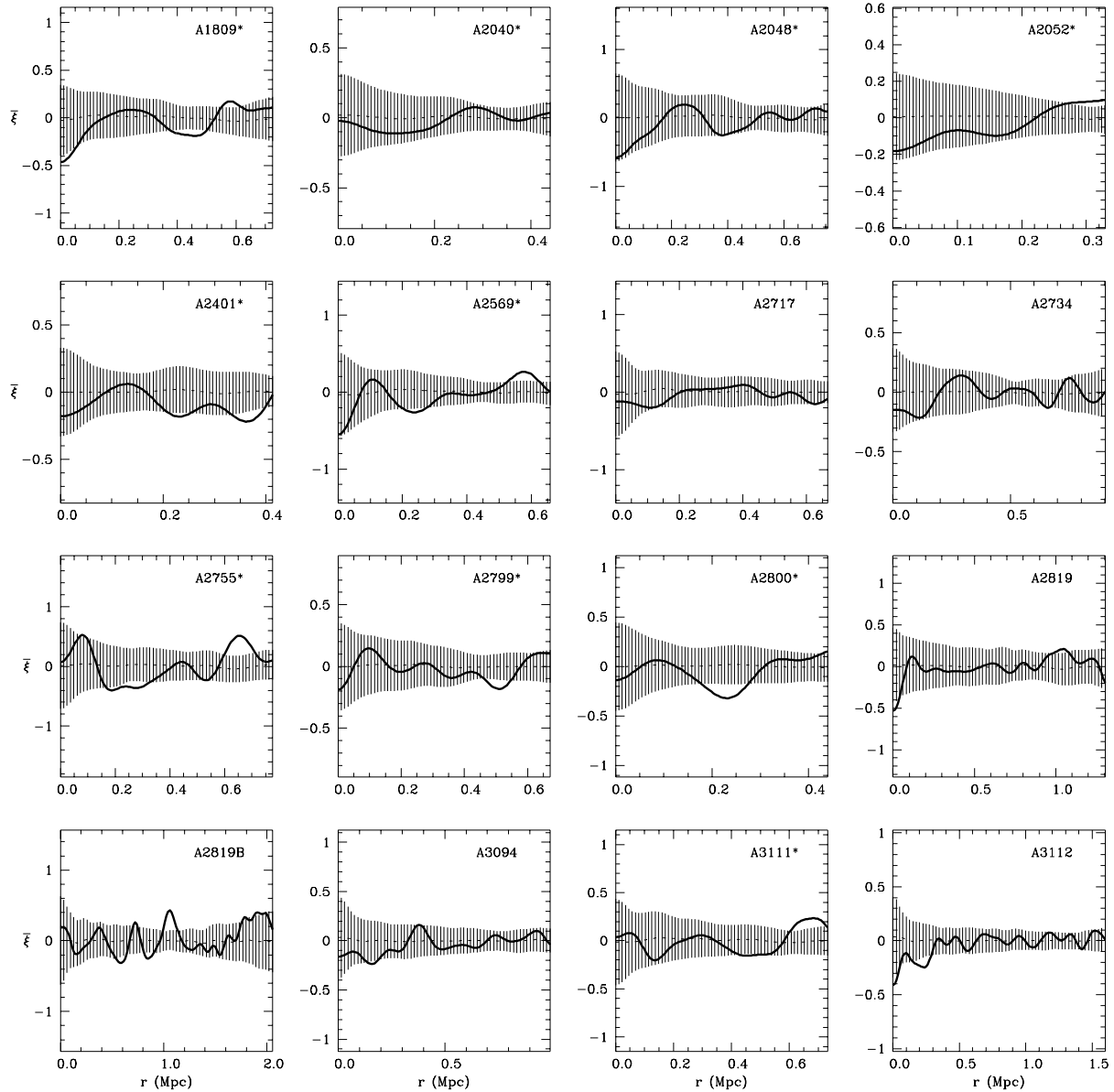
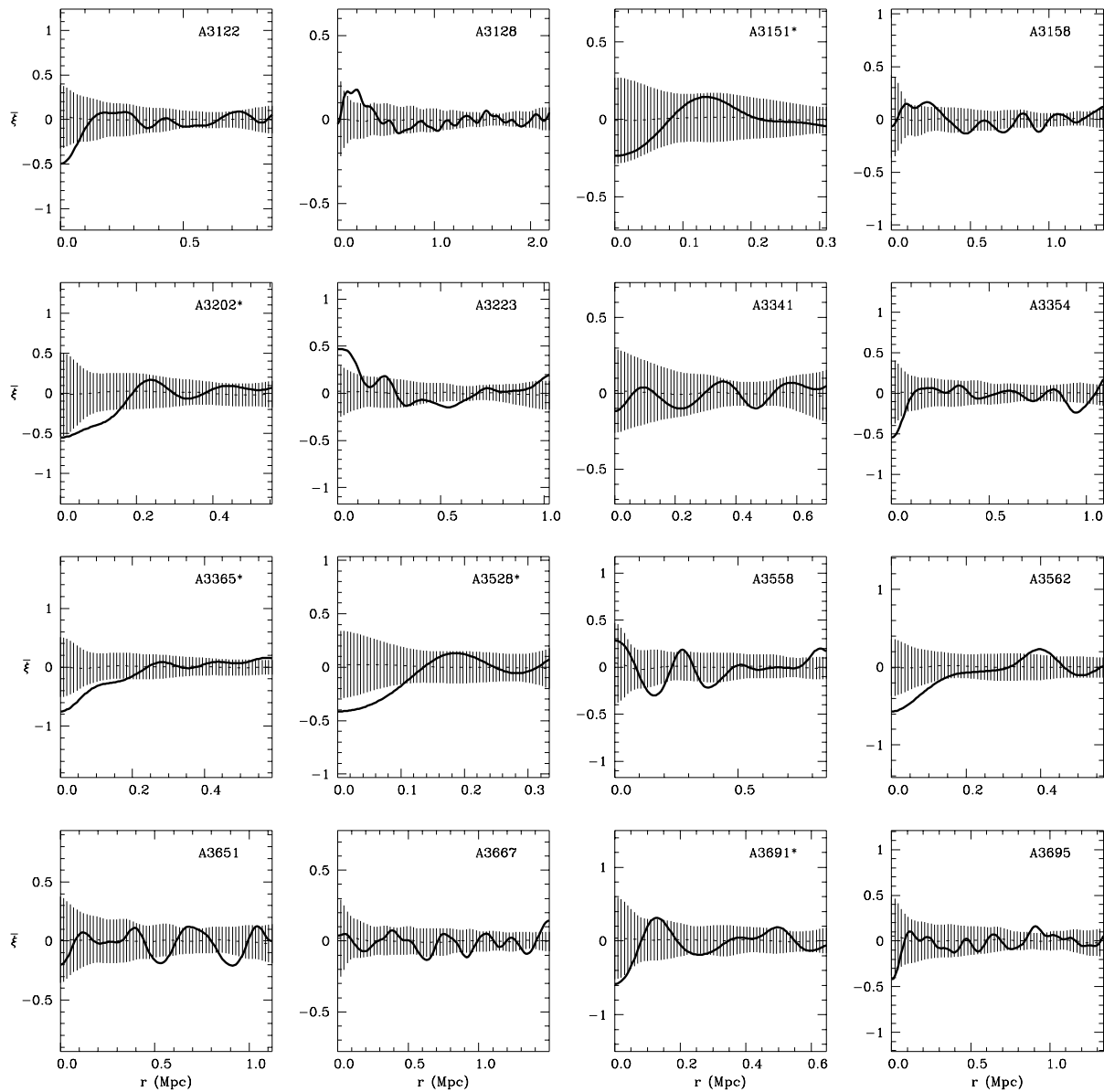


Fig. 1. (continued)

excluded). In this earlier study *all* systems gave positive central values of $\bar{\xi}$ and nine showed departures between 1 and 2σ at separations inferior to $0.2 h^{-1}\text{Mpc}$. The only cluster in common between both investigations, Abell 754, is found here to exhibit no evidence for substructure, yet in Sa93 this cluster was seen to produce, with a similar number of objects, a strong positive central signal. One plausible origin of that conflict could be the very different areal coverage of the galaxy samples used in the two studies for this particular cluster (see Fig. 2; but notice that the orientations, ellipticities and barycenter positions are, nevertheless, in very good agreement). This would be the case if the positive detection in Sa93 was produced by

small subgroups located outside the cluster core. We also point out the suggestion made in Sa93 that the asymmetry shown by the projected galaxy distribution in the Dressler & Shectman's field, not noticeable at short distances from the cluster center, could have caused the observed signal.

It is interesting to note that similarly strong discrepancies can be observed with respect to the results of the wavelet analysis of substructure performed by Escalera et al. (1994). These authors found that only three systems among the 16 that they investigated, most of them Dressler & Shectman's clusters, did not show significant small-scale subclustering. Further, there is a good agree-


Fig. 1. (continued)

ment between the results of this study and of Sa93 for the common clusters.

Finally, it is also worth noting that, with the exception of the system A0151, the remaining five clusters with evidence for small-scale structure in the galaxy positional data show also signs of substructure in velocity space (see Table 1).

5. Summary and discussion

We have evaluated here the frequency of subclustering in 67 well-sampled nearby rich galaxy clusters extracted from the list of 220 compact redshift systems identified

in the homogeneous ENACS catalog. Three classical diagnostics sensitive to correlations in velocity space have registered amounts of substructure comparable with those found in earlier studies which applied the same estimators to datasets less representative of the nearby rich cluster population. The average two-point correlation function statistic has allowed us to investigate the clumpiness of the two dimensional galaxy distributions at small intergalactic separations. In doing so we have found that only about one of every 10 systems studied shows evidence for positive correlation among the projected positions of its member galaxies at scales inferior to $0.2 h^{-1} \text{Mpc}$. This result contrasts markedly with the very high fraction of Dressler &

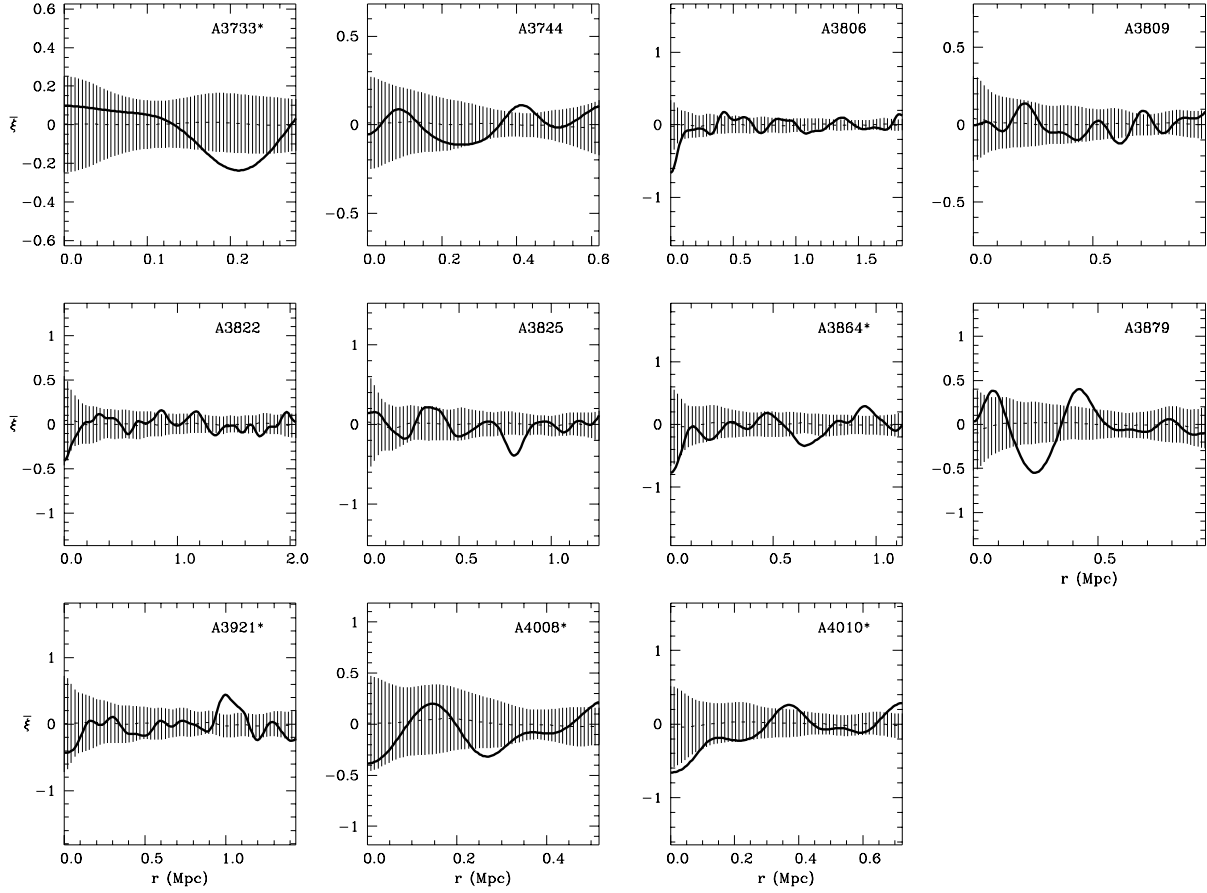


Fig. 1. (continued)

Schechter's clusters which demonstrated signs of small-scale substructure in the earlier analysis by Sa93 (see also Escalera et al. 1994).

It is possible that already mentioned factors such as cluster selection biases, likely affecting some of the existing catalogs, or the restricted coverage of the galaxy distributions of part of the clusters studied here may be partially responsible for this conflicting result. Nevertheless, there are grounds for believing that it could be caused too by an increase of the incompleteness of the ENACS galaxy samples at small scales. A telling argument in support of this latter viewpoint is that 25 of the 28 magnitude-limited single-plate systems (and 21 of the 31 multiple-plate ones) for which the $\bar{\xi}$ statistic has been inferred exhibit negative central values of this function. Since in the absence of correlation among galaxy positions positive and negative values of $\bar{\xi}(0)$ are equally probable (see Sa93), we infer that the ENACS clusters do show suggestive evidence of a systematic deficiency of galaxies at very short separations.

What then could have originated this effect? Let us remember that the ENACS project was aimed to obtain extensive redshift data in the fields of more than 100

rich galaxy clusters. To achieve this goal in a reasonable amount of time the number of exposures for each targeted cluster was minimized, making it difficult to compensate the operational restrictions inherent to the fiber-optic system (limited number of fibers available, minimum distance allowed for the positioning of contiguous fibers, etc) with redundant exposures. This might well have affected the reproduction of the finest details of the cluster galaxy distributions, especially when the coverage was done by means of a single plate. Notice, in this regard, that only one single-plate cluster is among the 6 systems that show signs of small-scale substructure in our dataset. (One may wonder if this latter result could have been produced instead by the relatively small galaxy populations of the single-plate clusters; this possibility is challenged, however, by the fact that in Sa93 seven of the 9 systems which gave a positive detection had less than 50 objects.) The reduced success in the redshift measurement for the brightest galaxies (see Sect. 2, and Katgert et al. 1996), which are fair tracers of substructures within clusters (Biviano et al. 1996; Gurzadyan & Mazure 1998) is another factor

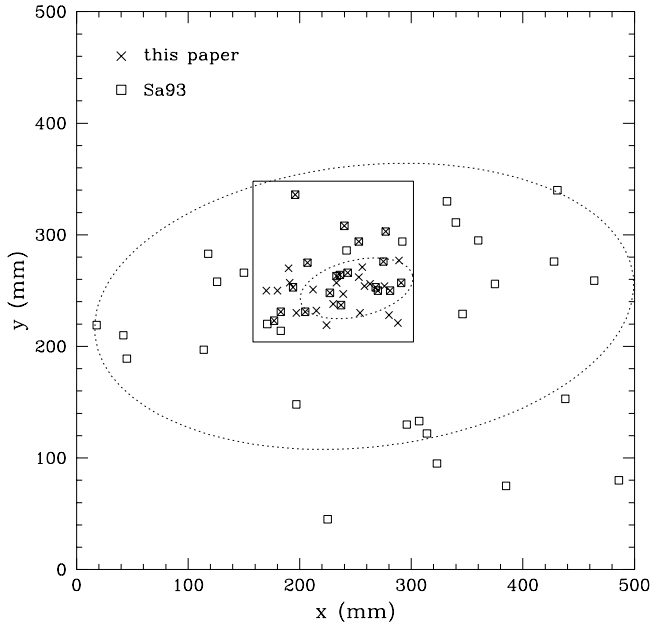


Fig. 2. Superposition of the galaxy plots corresponding to the magnitude-limited samples of the cluster Abell 754 defined in the present study and in Sa93. Likely members of the two datasets are identified by diagonally-crossed open squares. The inner square delimits the area used here for the ENACS data. The dotted ellipses inscribed within each field encompass the objects that participate in the calculation of $\bar{\xi}(s)$. Coordinates are in millimeters (scale $10''9 \text{ mm}^{-1}$).

which may have also contributed to conceal the presence of small subgroups.

To sum up, the amount of intermediate and large-scale subclustering detected in the ENACS systems is in fair agreement with, and therefore validates, the results of previous analysis of substructure in nearby rich clusters based on less homogeneous datasets. The present investigation, however, has revealed that the ENACS galaxy samples could suffer from an increasing incompleteness towards small intergalactic separations. In this regard, we caution that the ENACS data by themselves may be insufficient in applications requiring a detailed description of the small-scale substructuring properties of clusters, such as those that investigate the formation of these systems and its consequences on cosmological theories.

Acknowledgements. The authors would like to thank Peter Katgert for enlightening and useful discussions. GGC acknowledges support by the Universitat Politècnica de Catalunya, through research contract PR97-07. This work has been supported by the Dirección General de Investigación Científica y Técnica, under contract PB96-0173.

References

- Abell, G.O., Corwin, H.G. Jr., Olowin, R.P., 1989, *ApJS* 70, 1 (ACO)
- Adami, C. Mazure, A., Katgert, P., Biviano, A., 1998, *A&A* 336, 63
- Beers, T.C., Forman, W., Huchra, J.P., Jones, C., Gebhardt, K., 1991, *AJ* 102, 1581
- Bird, C.M., 1994, *AJ* 107, 1637
- Bird, C.M., Beers, T.C., 1993, *AJ* 105, 1596
- Biviano, A., Durret, F., Gerbal, D., et al., 1996, *A&A* 311, 95
- Biviano, A., Katgert, P., Mazure, A., et al., 1997, *A&A* 321, 84
- Davis, D.S., Bird, C.M., Mushotzky, R.F., Odewahn, S.C., 1995, *ApJ* 440, 48
- Dressler, A., Shectman, S.A., 1988a, *AJ* 95, 985 (DS88)
- Dressler, A., Shectman, S.A., 1988b, *AJ* 95, 284
- Escalera, E., Biviano, A., Girardi, M., et al., 1994, *ApJ* 423, 539
- Fitchett, M.J., Webster, R.L., 1987, *ApJ* 317, 653
- Geller, M.J., Beers, T.C., 1982, *PASP* 94, 421
- Girardi, M., Escalera, E., Fadda, D., et al., 1997, *ApJ* 482, 41
- Gurzadyan, V.G., Mazure, A., 1998, *MNRAS* 295, 177
- Jones, C., Forman, W., 1992, in *Clusters and Superclusters of Galaxies*, ed. A.C. Fabian (Dordrecht: Kluwer), 49
- Katgert, P., Mazure, A., Perea, J., et al., 1996, *A&A* 310, 8
- Katgert, P., Mazure, A., den Hartog, R., et al., 1998, *A&AS* 129, 399
- Kogut, A., Lineweaver, C., Smoot, G.F., et al., 1993, *ApJ* 419, 1
- Malumuth, E.M., Kriss, G.A., Van Dyke Dixon, W., Ferguson, H.C., Ritchie, C., 1992, *AJ* 104, 495
- Mazure, A., Katgert, P., den Hartog, R., et al., 1996, *A&A* 310, 31
- Mohr, J.J., Fabricant, D.G., Geller, M., 1993, *ApJ* 413, 492
- Rhee, G.F.R.N., van Haarlem, M.P., Katgert, P., 1991, *A&A* 246, 301
- Salvador-Solé, E., Sanromá, M., González-Casado, G., 1993a, *ApJ* 402, 398
- Salvador-Solé, E., González-Casado, G., Solanes, J.M., 1993b, *ApJ* 410, 1 (Sa93)
- Serna, A., Gerbal, D., 1996, *A&A* 309, 65
- Teague, P.F., Carter, D., Gray, P.M., 1990, *ApJS* 72, 715
- West, M.J., Bothun, G.D., 1990, *ApJ* 350, 36
- West, M.J., Oemler, A.Jr., Dekel, A., 1988, *ApJ* 327, 1
- Yee, H.K.C., Ellingson, E., Carlberg, R.G., 1996, *ApJS* 102, 269
- Zabludoff, A.I., Huchra, J.P., Geller, M.J., 1990, *ApJS* 74, 1